**THE EUROPEAN
PHYSICAL JOURNAL D**

Regular Article

Impact of fiber birefringence on correlated photon pair generation in highly nonlinear microstructure fibers

W. Zhang[a], Q. Zhou, J.R. Cheng, Y.-D. Huang, and J.D. Peng

Room 113, Wei Qing Building, Department of Electronic Engineering, Tsinghua University, 100084 Beijing, P.R. China

Abstract. In this paper, correlated photon pair generation in a piece of highly nonlinear microstructure fiber with birefringence is investigated experimentally under different pump polarization directions. In the experimental condition, correlated photon pairs are generated by two independent scalar scattering processes along the two fiber polarization axes. Under linearly polarized pump light with a polarization direction of $45°$ with respect to the fiber polarization axes, the polarization entangled characteristics of generated two-photon state is demonstrated. The two-photon interference fringes are measured with fringe visibilities of $96 \pm 3\%$ and $87 \pm 4\%$ under two non-orthogonal detecting polarization directions at signal side. The experimental results are discussed using the quantum theory of spontaneous parametric fluorescence in birefringent fibers, showing that the pump polarization dependence of correlated photon pair generation in the highly nonlinear microstructure fiber is due to its group birefringence. The experiment and theoretical analysis show that fiber birefringence has important impact on correlated photon pair generation, which provides a simple way to generate maximum polarization entanglement in fibers.

1 Introduction

Operating in low loss transmission window of commercial silica fibers, 1.5 μm correlated photon pair sources have important applications in quantum communication and quantum information process over large geographical scale [1,2]. Correlated photon pair generation in fibers by spontaneous parametric fluorescence provides a promising way to realize efficient, compact and all fiber correlated photon pair sources, which attracts much attention due to their compatibility with current optical fiber networks [3–5]. Thanks to their high nonlinearity and flexibility in dispersion design, highly nonlinear microstructure fibers (HN-MSFs) have been proven as important candidates for this application. Compared with traditional dispersion shifted fibers used in previous experiments, the fiber length can be shortened from hundreds of meters to several meters for the high nonlinear characteristics of HN-MSFs, [6–10]. On the other hand, correlated photon pair generations at 800 nm band and 800 nm/1.5 μm are realized in HN-MSFs respectively [11,12], utilizing their unique dispersion characteristics. The former is a potential competitor with correlated photon pair sources based on spontaneous parameter down conversion in nonlinear crystals. The latter provides a new way to realize all fiber 1.5 μm band heralded single photon sources, which have important applications in quantum key distribution systems.

In most experiments of fiber based correlated photon pair generation, the impact of fiber birefringence is not considered. In some of them, fibers with low birefringence are used, while in others, photon pairs are generated along one fiber polarization axis to avoid the impact of fiber birefringence. Recently, theories of spontaneous parametric fluorescence in birefringent fibers are developed [13], showing that four spontaneous parametric processes should be considered in birefringent fibers. In two of them, two pump photons are annihilated and a photon pair is generated along the same fiber polarization axis (scalar scattering process), while in the other two, two annihilated pump photons and the generated photon pair are along two orthogonal fiber polarization axes (vectorial scattering process). Theoretical analysis shows that the fiber birefringence can extend the two-photon state of the generated photon pairs. HN-MSFs have non-neglected birefringence, induced unavoidably in their fabrication process [14]. Hence, the impact of fiber birefringence is unavoidable in HN-MSFs based correlated photon pair generation. An experiment generating cross polarized photon pairs at 800 nm has been reported [15], in which the impact of pump pulse delay between the two fiber polarization axes is discussed. However, the impact of fiber birefringence on the spontaneous parametric fluorescence and the two-photon state of generated photon pairs has not been explored experimentally.

In this paper, the impact of birefringence on the nonlinear parametric processes in fibers is shown by the amplified parametric fluorescence spectra in the HN-MSF

[a] e-mail: `zwei@mail.tsinghua.edu.cn`

Table 1. Parameters of the HN-MSF used in the experiment.

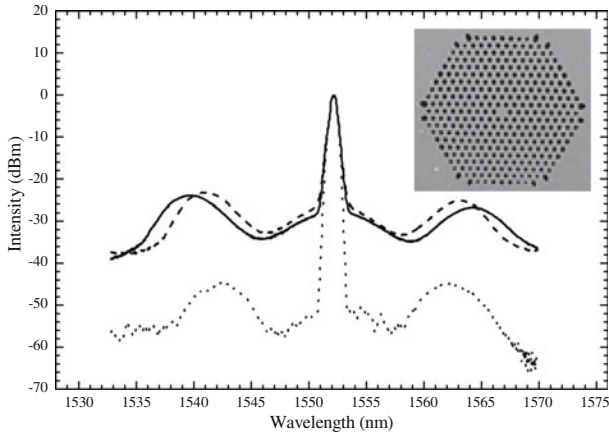|	
Nonlinear coefficient	66.7 /W/km
Phase birefringence (Δn)	3.5×10^{-5}
Group birefringence	0.158 ps/m
Dispersion of the two polarization axes at 1552.8 nm	7.5 ps/km/nm
(the pump wavelength in the experiment)	9.8 ps/km/nm
Zero dispersion wavelengths of the two polarization axes	1563.4 nm
	1564.8 nm

Fig. 1. Amplified parametric fluorescence spectra in the HN-MSF under different pump polarization directions. Solid and dashed lines: fluorescence spectra when pump lights are polarized along the two fiber polarization axes, respectively; dotted line: fluorescence spectrum when pump light is polarized along the direction 45° to the two fiber polarization axes; inset: SEM image of the HN-MSF used in the experiment.

under different pump polarizations firstly. Then, 1.5 μm correlated photon pairs are generated in the HN-MSF by an experiment setup based on commercial fiber components. The characteristics of the generated photon pairs under different pump light polarization directions are investigated experimentally, showing that they are contributions of two independent scalar scattering processes along the two fiber polarization axes and their two-photon state shows characteristics of polarization entanglement. The content is structured as follows: the amplified parametric fluorescence spectra in the HN-MSF under different pump polarizations is shown in Section 2, followed by the experiment results of 1.5 μm correlated photon pair generation in Section 3. Section 4 provides a theoretical discussion of the generated two-photon state under our experiment condition. The conclusion is presented in Section 5.

2 Birefringence in the HN-MSF and its impact on the amplified parametric fluorescence spectra

The HN-MSF used in the experiment (fabricated by Crystal fiber A/S Inc.) is 25 m in length. It has triangle hole array structure, as shown in the inset of Figure 1. The diameters of the silica core and air holes are 1.8 μm and 0.89 μm, respectively. It has two zero dispersion wavelengths, one of them is 1565 nm (provided by the manufacturer). In our previous work, its nonlinear coefficient [16] and parameters of fiber dispersion and birefringence [17] in 1.5 μm band have been measured, listed in Table 1.

To observe the amplified parametric fluorescence, pump lights with high power level should be injected into the HN-MSF. The pump light is generated by a pulsed light source with a master oscillator power amplifier configuration, including a continuous wave distributed feedback semiconductor laser at 1552.8 nm, an external modulator and an erbium doped fiber amplifier (EDFA). The frequency, pulse width and peak power of the pump pulse series are 1 MHz, 10 ns and 5 W, respectively. A polarization controller is used to ensure the pump light in linear polarization, while its polarization direction is adjusted by a half wave plate before the HN-MSF. The fluorescence spectra are observed by an optical spectrum analyzer (Agilent 86142B), shown in Figure 1.

Figure 1 shows that the fluorescence spectrum varies obviously with polarization direction of the pump light, which could not be expected in a fiber without birefringence. At a certain pump polarization direction, the fluorescence intensity reaches its maximum. Rotating the pump polarization direction, the fluorescence intensity reduces rapidly and reaches its minimum when the rotated angle of pump polarization direction is 45°, then it increases and reaches another maximum when the rotation angle is 90°. The difference between the intensity maximum and minimum is higher than 20 dB. This obvious pump polarization dependence shows that the amplified parametric fluorescence is generated by two independent scalar parametric processes along the two fiber polarization axes, whose intensities grow exponentially with pump polarization components along the two axes respectively if the phase matching conditions are satisfied [13]. The pump polarization direction corresponding to the maximum fluorescence intensity is along one of the fiber polarization axes.

The intensity variation of amplified parametric fluorescence with the pump polarization shows that birefringence in the HN-MSF is sufficient to bring obvious impact on the nonlinear parametric processes in the fiber. It can be expected that if the pump power level are reduced, correlated photon pairs would be generated by spontaneous parametric fluorescence based on the two independent scalar parametric processes, i.e. the two scalar scattering processes mentioned in reference [13]. Hence, they should have a superposed two-photon state and show
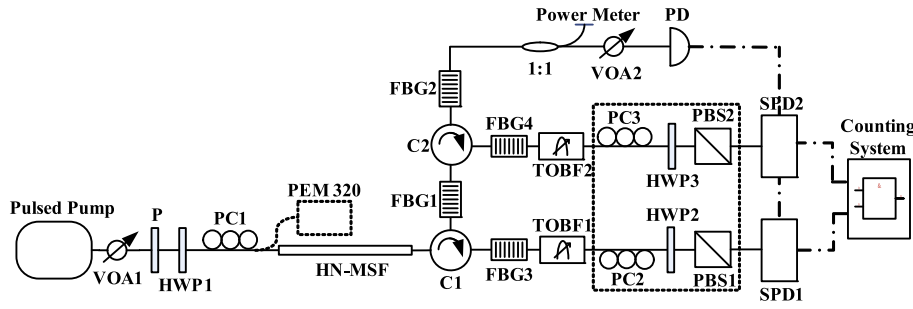
Fig. 2. (Color online) Experimental setup.

characteristics of polarization entanglement. If the pump polarization components along the two fiber polarization axes have the same power, maximum polarization entanglement could be expected, which is demonstrated experimentally in Section 3.

3 1.5 μm correlated photon pair generation in the HN-MSF under different pump polarization directions

3.1 Experimental setup

The experimental setup is shown in Figure 2, based on commercial fiber components. The pulsed pump light is generated from a passive mode locked fiber laser. A filter based on a fiber Bragg grating and a circulator is used to extend its pulse width by narrowing its spectrum. Then it is amplified by an EDFA. Amplified spontaneous emission of the EDFA is suppressed by a filter system based on a tunable optical band-pass filter, a fiber Bragg grating and a circulator, achieving a side-band suppression of 115 dB at wavelengths where the signal and idler photon detection is performed. The center wavelength, line width and repeating frequency of the pulsed pump light are 1552.75 nm, 0.2 nm and 1 MHz, respectively. The pulse width is several tens of pico-seconds, estimated by the pump line width. Before it injects into the HN-MSF, a variable optical attenuator (VOA1) is used to control its power level, while a polarizer (P), a rotatable half-wave plate (HWP1) and a polarization controller (PC1) are used to achieve linear polarization and adjust its polarization direction.

1.5 μm correlated photon pairs are generated when pump pulses pass through the HN-MSF. Since the photon number in a pump pulse is far larger than the number of generated photon pairs, high pump photon suppression is required for signal and idler photon detection. Hence, photon pairs generated in the HN-MSF are directed into two single photon detectors through a filtering and splitting system based on fiber Bragg gratings (FBG1 ∼ 4), circulators (C1, C2) and tunable optical band-pass filters (TOBF1, TOBF2). The center wavelength and spectral width of selected signal photons are 1549.9 nm and 0.2 nm, respectively, while 1555.6 nm and 0.2 nm for the idler ones. The total pump suppression is higher than 105 dB

at both of the signal and idler wavelengths. The two single photon detectors (SPD1, SPD2, Id201, Id Quantique) are based on InGaAs/InP avalanche photodiodes. The SPD1 and SPD2 are for the signal and idler photons, respectively. They are operated in gated Geiger mode with a detection time window of 2.5 ns, triggered by the residual pump light using an optical detector (PD).

3.2 Correlated photon pair generation in the HN-MSF

Four photon count rates are measured in the experiment. The single-side photon count rates of signal and idler photons are denoted by N_s and N_i respectively. N_{co} denotes the coincident count rate, representing the result that both single photon detectors record photons simultaneously and the detected photons are generated by the same pump pulse. On the other hand, N_{ac} denotes the rate that both single photon detectors record photons generated by different pump pulses, called accidental coincidence count rate. N_{co} and N_{ac} can be measured by a count system with a coincident logic circuit. All the experimental data are obtained under a photon count time of 30 s.

Firstly, correlated photon pair generation is demonstrated when the pump light polarized along one of the fiber polarization axes. In this case, only one scalar scattering process would take place. Figure 3 shows the measured single-side photon count rates at the signal side and idler side. A second-order polynomial, N_s, $N_i = s_1 N_p + s_2 N_p^2$, is used to fit the experimental data (the solid line), in which s_1 and s_2 are the linear and quadratic fitting coefficients, N_p is the pump photon number per pulse, the quadratic term represents the contribution of spontaneous parametric fluorescence. Experimental results shows $s_1 = 1.79$ and $s_2 = 1.865$ for the signal side, while $s_1 = 0.8478$ and $s_2 = 0.8883$ for the idler side, showing that photons detected in either side have the contribution of spontaneous parametric fluorescence.

Figure 4a shows the coincident and accidental coincident count rates with increasing signal side photon count rates. It can be seen that the coincident count rates are obviously higher than the accidental coincident rates, demonstrating the quantum correlation of generated signal and idler photons. To show this more clearly, the ratio between them is shown in Figure 4b. The maximum ratio in our experiment is 5.3 under a low pump level, similarly
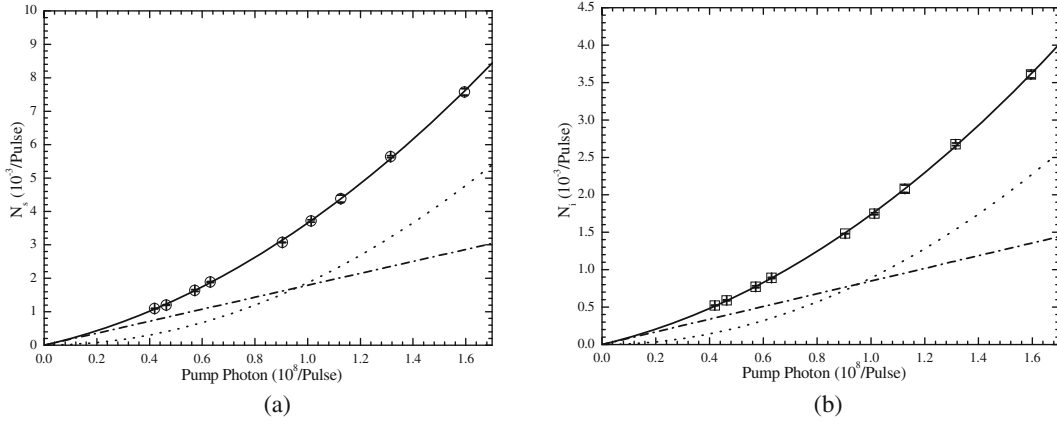
Fig. 3. Single side photon count rates under different pump level when the pump light polarized along one of the HN-MSF polarization axes: (a) signal side results; (b) idler side results. The solid lines are the fit curves of N_s, $N_i = s_1 N_p + s_2 N_p^2$. The dotted lines and dash-dotted lines are the linear and quadratic terms, respectively.
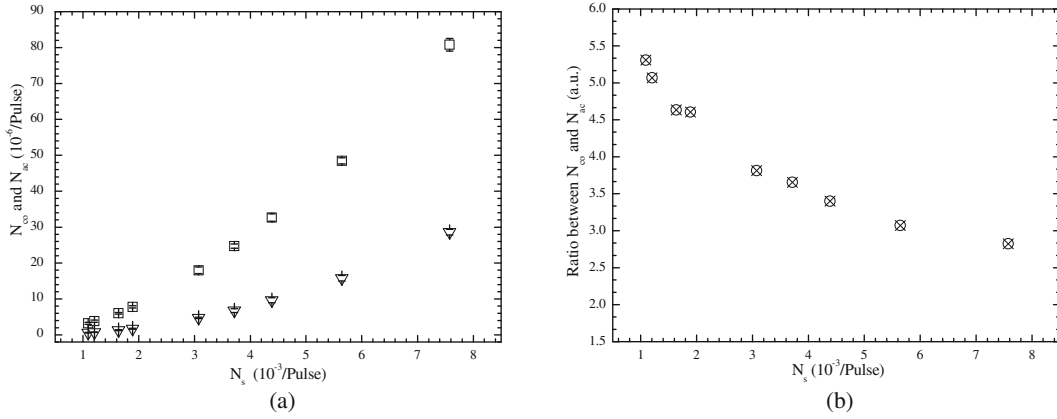

Fig. 4. The coincident and accidental coincident count rates with increasing signal side photon count rates: (a) the coincident (the square dots) and accidental coincident (the triangular dots) count rates; (b) the ratio between them.

with previous works of fiber based 1.5 μm correlated photon pair generation in room temperature [3]. The limited maximum ratio is due to the contribution of noise photons without quantum correlation characteristics, represented by the linear term in Figure 3.

To investigate the impact of HN-MSF birefringence on correlated photon pair generation, the influence of noise photons should be removed. In our experiment, the four measured photon count rates can be expressed as

$$
\begin{aligned}
N_s &= \eta_s(R + R_s) + d_s \\
N_i &= \eta_i(R + R_i) + d_i \\
N_{co} &= \eta_s\eta_i(R + RR_s + RR_i + R_sR_i) \\
&\quad + \eta_s(R + R_s)d_i + \eta_i(R + R_i)d_s \\
N_{ac} &= \eta_s\eta_i(R^2 + RR_s + RR_i + R_sR_i) \\
&\quad + \eta_s(R + R_s)d_i + \eta_i(R + R_i)d_s,
\end{aligned} \tag{1}
$$

where R is the generation rate of correlated photon pairs by spontaneous parametric florescence; R_s and R_i are generation rates of noise photons on the signal and idler side, respectively, which are mainly due to spontaneous Raman scattering. Another noise contribution is dark count rates of the two single photon detectors, which are denoted by

d_s and d_i for the SPD1 and SPD2 respectively. The photon count rates are also influenced by collection efficiencies of signal and idler photons, including detection efficiencies of the two single photon detectors and losses of the filtering and splitting system before them. They are denoted by η_s and η_i for the signal and idler photons, respectively. Since dark count rates and collection efficiencies have been measured during the experiment setup preparation ($\eta_s = 3.36\%$, $\eta_i = 2.38\%$, $d_s = 5.98 \times 10^{-5} \pm 1.001 \times 10^{-6}$ and $d_i = 4.67 \times 10^{-5} \pm 0.999 \times 10^{-6}$), R, R_s and R_i can be calculated from experimental results of the four count rates according to equation (1), shown in Figure 5. It can be seen that, R increases with pump level quadratically, while, R_s and R_i increases with pump level linearly. In the following section, the impact of HN-MSF birefringence on R is investigated experimentally.

3.3 Impact of birefringence on correlated photon pair generation in the HN-MSF

By rotating HWP1 before the HN-MSF, four photon count rates are measured under linearly polarized pump lights with different polarization directions and the same pump
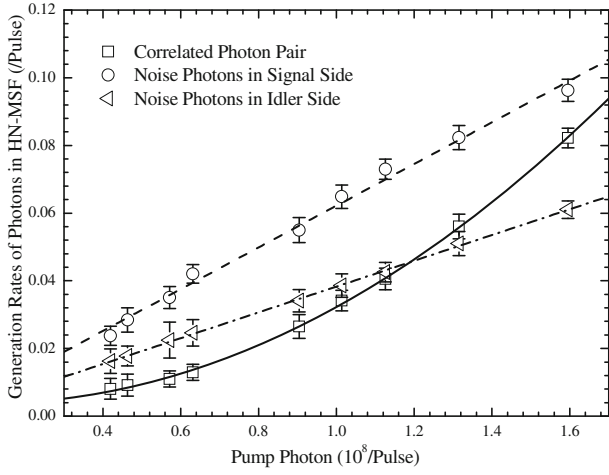
Fig. 5. Generation rates of photons in HN-MSF. The square, triangular, and circular dots represent results of correlated photon pairs, noise photons at idler side and noise photons at signal side. The solid, dash-dotted and dashed lines are their fitting curves.

Fig. 6. Generation rates of correlated photon pairs under different pump polarization directions.

power. The generation rate of the correlated photon pairs, R, is calculated and normalized, shown in Figure 6. It can be seen that R varies with the pump polarization direction obviously, reaching its maximum when the pump polarization direction is along the two polarization axes of the HN-MSF, while, reaching its minimum when the angle between the pump polarization direction and one of the fiber polarization axes, which is denoted by θ, is 45°. It can be fitted by a sine curve between 0.5 and 1 with a period of 90°.

This result reflects the impact of birefringence on correlated photon pair generation in the HN-MSF. When $\theta \neq 0$ and 90°, the pump light is decomposed into two polarization components along the two fiber polarization axes. Both scalar scattering processes and vectorial scattering processes would take place, generating correlated photon pairs in different two-photon states. However, wavelengths of photon pairs generated by the scalar and vectorical scattering processes would be different due to the birefringence in HN-MSF. In our experiment, detected signal and idler photons are selected by narrow band filters, whose center wavelengths close to the pump wavelength, where scalar scattering processes are dominant. Hence, the detected correlated photon pairs are generated through two independent scalar scattering processes along the two fiber polarization axes respectively. The relation between R and θ should be $R \propto \sin^4 \theta + \cos^4 \theta = 1 - 0.5 \sin^2(2\theta)$, considering the pump light polarization decomposition and that the generation rate of correlated photon pairs by one scalar scattering process increases quadratically with the pump level, which is shown in Figure 5. It is exactly the fitting sine curve in Figure 6.

A direct conclusion of the above analysis is that the generated photon pairs should be polarization entangled when $\theta \neq 0$ and 90°. Especially, when $\theta = 45°$, the two pump polarization components along two fiber polarization axes have the same power, leading to a
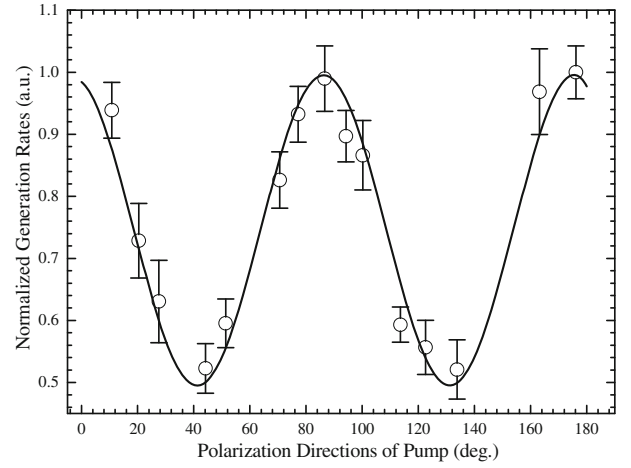
maximally polarization entangled state in the form of $\frac{1}{\sqrt{2}} \left(|x_s\rangle |x_i\rangle + e^{i\alpha} |y_s\rangle |y_i\rangle \right)$, where x and y denote the two polarization axes of the HN-MSF, s and i denote the signal and idler, respectively. α is an arbitrary phase. The polarization entangled characteristics of the two-photon state is demonstrated experimentally, by inserting polarization analyzer systems before the two SPDs shown in the dashed square in Figure 2, which are composed of polarization controllers (PC2, PC3), half-wave plates (HWP2, HWP3) and polarization beam splitters (PBS1, PBS2).

Firstly, the pump polarization direction is set along one of the fiber polarization axes and the PC2 and PC3 are adjusted to achieve the maximum single-side count rates of the signal and idler sides respectively. In this case, the detected signal and idler photons are generated by the scalar scattering process along this fiber polarization axis. Then, the pump polarization direction is set as $\theta = 45°$, while the states of PC2 and PC3 are unchanged. The four photon count rates are measured as the HWP2 at signal side and HWP3 at idler side are rotated to different angles, which is equivalent to rotate the detectable polarization directions of signal and idler sides. The double angle of the HWP3 rotation is θ_i, defined as the detecting angle at idler side, while, the double angle of the HWP2 rotation is θ_s, defined as the detecting angle at signal side. Figure 7 shows the experimental results.

Figure 7a is the coincident count per 30 s (accidental coincident count has been subtracted) under different θ_i. Circular and square dots are the experiment data when θ_s is set to 0 and 135°, respectively. Solid and dashed lines are the fitting curves, showing that the fringe visibilities of two photon interference are $96 \pm 3\%$ and $87 \pm 4\%$ for $\theta_s = 0$ and 135°, respectively. The inset of Figure 7b shows the photon count (square dots) of the idler side under different θ_i and the contributions of noise photons (circular dots) mainly generated by spontaneous Raman scattering, calculated by equation (1). It shows that the idler
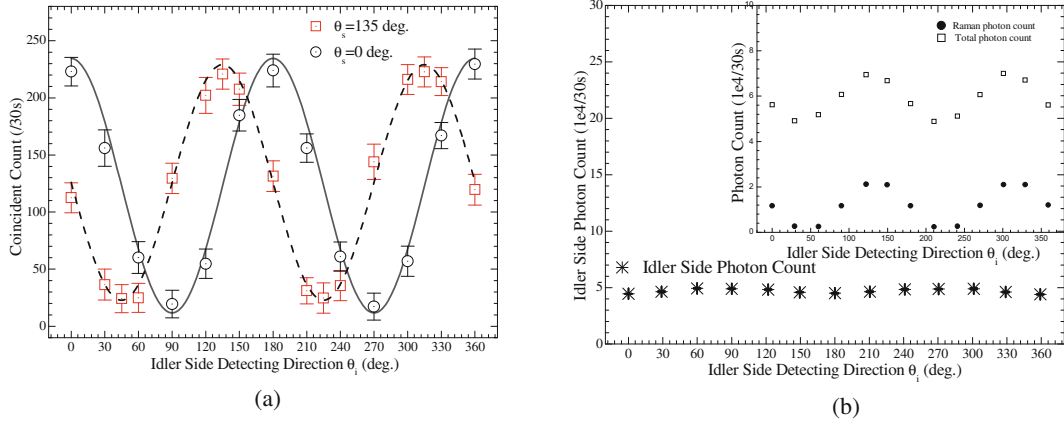
Fig. 7. (Color online) Experimental results under different idler detecting angles: (a) two photon interference fringes; (b) idler side photon count.

side photon count varies with θ_i due to the noise photons, which are mainly co-polarized with the pump light, [21]. Subtracting the contribution of noise photons from the idler side photon count results, the contribution of photon pairs can be calculated and shown in the main figure of Figure 7b. It is almost unchanged with θ_i, showing the single side polarization indistinguishableness of the photon pairs. Hence, the experiment results demonstrate that the photon pairs generated in the HN-MSF with birefringence under $\theta = 45°$ have the characteristics of maximum polarization entanglement.

4 Discussion

Above experiment results can be explained by the quantum theory of spontaneous parametric fluorescence in birefringent fibers, [13]. In the case of $\theta = 45°$, the photon flux spectral density of the two-photon states generated by scalar scattering processes and vectorial scattering processes are

$$|\xi_{xx}(L,\Omega)|^2 = |\xi_{yy}(L,\Omega)|^2 = \frac{(\gamma P_0 L)^2}{4}$$
$$\times \text{sinc}^2\left[\left(\beta_2\Omega^2 + \gamma P_0\right)\frac{L}{2}\right]$$

$$|\xi_{xy}(L,\Omega)|^2 = \frac{1}{9}(\gamma P_0 L)^2$$
$$\times \text{sinc}^2\left[\left(\Delta\beta_1\Omega + \beta_2\Omega^2 + \gamma P_0\right)\frac{L}{2}\right]$$

$$|\xi_{yx}(L,\Omega)|^2 = \frac{1}{9}(\gamma P_0 L)^2$$
$$\times \text{sinc}^2\left[\left(\Delta\beta_1\Omega - \beta_2\Omega^2 - \gamma P_0\right)\frac{L}{2}\right] \quad (2)$$

Where, Ω is the frequency detune between the pump light and the signal/idler photons. P_0 is the total pump power. γ is the fiber nonlinear coefficient and L is the fiber length. $\Delta\beta_1$ and β_2 are the fiber group birefringence and group velocity dispersion at the pump wavelength, respectively.
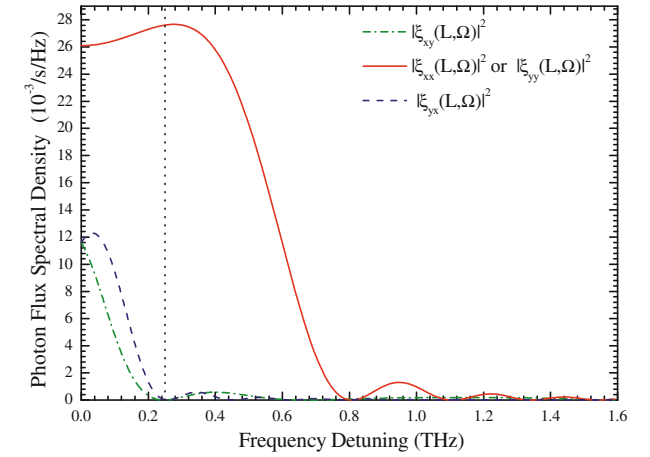

Fig. 8. (Color online) Photon flux spectral densities of the scalar and vectorial scattering processes in the HN-MSF under experimental condition.

The photon flux spectral density of different processes are calculated and shown in Figure 8 based on parameters of the HN-MSF (shown in Tab. 1, neglecting the polarization dependent dispersion by using the average dispersion at the pump wavelength) and experimental setup (the fiber is 25 m long, the peak pump power is 0.5 W). The frequency detune of the narrow band filters is 0.25 THz, marked as the dotted line in Figure 8. It can be seen that the two scalar scattering processes are dominant at the frequency detune of the filter used in the experiment, agreeing well with experiment results.

Equation (2) shows that the difference of photon flux spectral densities between scalar and vectorial scattering processes comes from the group birefringence of the HN-MSF, which impacts the phase-matching condition of the vectorial scattering processes. To show it more clearly, the ratios of photon flux spectral densities between vectorial and scalar scattering processes under increasing group birefringence are calculated and shown in Figure 9. Figures 9a and 9b are results under $\Omega = 0.25$ THz and $\Omega = 0.2763$ THz respectively, the former
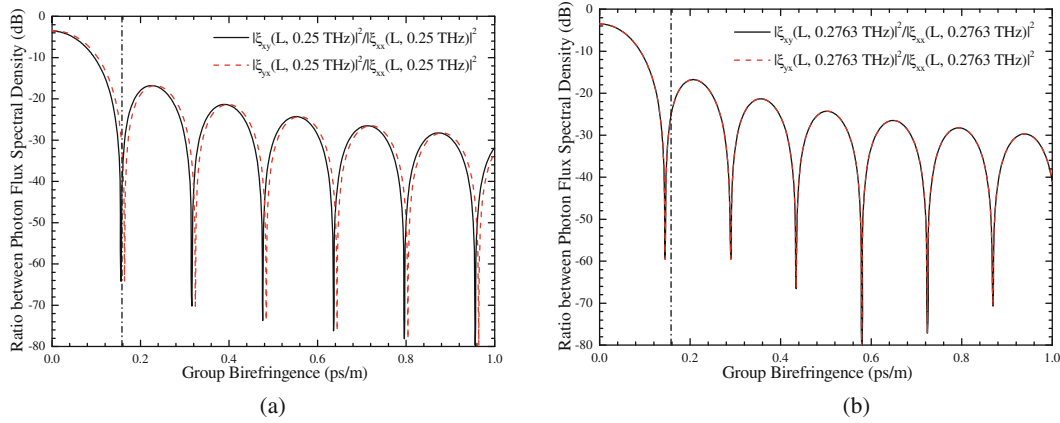
Fig. 9. (Color online) Ratios of photon flux spectral densities between vectorial and scalar scattering processes under increasing group birefringence: (a) $\Omega = 0.25$ THz and (b) $\Omega = 0.2763$ THz.

is the frequency detune of narrow band filters used in the experiment, the latter is the frequency detune satisfying the phase-matching condition of scalar scattering processes. Other parameters used in the calculation are the same as Figure 8. It can be seen that the ratios are reduced rapidly with increasing group birefringence, indicating that vectorial scattering processes can be neglected if two conditions are satisfied. Firstly, the frequency detune of the filters should be in the sideband of scalar scattering processes near the pump wavelength. Secondly, the group birefringence should be large enough to reduce the intensities of vectorial scattering processes. The dash-dotted lines denote the group birefringence of the HN-MSF used in the experiment, showing that the ratios are lower than -26 dB in both case. If the narrow band filters are set to the frequency detune satisfying the phase-matching condition of scalar scattering processes, both ratios are determined by $\frac{4}{9}\sin c^2\left(\frac{\Delta\beta_1\Omega L}{2}\right)$ according to $\beta_2\Omega^2 + \gamma P_0 = 0$, shown in Figure 9b.

demonstrating that pump polarization dependence of the correlated photon pair generation is due to group birefringence of the HN-MSF. The experiment and theoretical analysis show that birefringence in HN-MSFs has important impact on correlated photon pair generation, which provides a simple way to realize maximum polarization entanglement.

5 Conclusion

In this paper, the pump polarization dependence of correlated photon pair generation in a piece of HN-MSF is investigated experimentally, showing that the correlated photon pairs are generated by two independent scalar scattering processes along two polarization axes of the HN-MSF. The polarization entangled characteristics of the generated two-photon state is demonstrated under the pump polarization direction of $\theta = 45°$. The two-photon interference fringes are measured with fringe visibilities of $96 \pm 3\%$ and $87 \pm 4\%$ under two non-orthogonal detecting polarization directions at signal side. The experiment results are discussed using the quantum theory of spontaneous parametric fluorescence in birefringent fibers,

References

1. N. Gisin, G. Ribordy, W. Tittel, H. Zbinden, Rev. Mod. Phys. **74**, 145 (2002)
2. C.H. Bennett, S.J. Wiesner, Phys. Rev. Lett. **69**, 2881 (1992)
3. M. Fiorentino, P.L. Voss, J.E. Sharping, P. Kumar, IEEE Photon. Technol. Lett. **14**, 983 (2002)
4. H. Takesue, K. Inoue, Opt. Express **13**, 7832 (2005)
5. X. Li, L. Yang, L. Cui, Z.Y. Ou, D. Yu, Opt. Lett. **33**, 593 (2008)
6. J. Fan, A. Migdall, L.J. Wang, Opt. Lett. **30**, 3368 (2005)
7. J. Sharping, J. Chen, X. Li, P. Kumar, R. Windeler, Opt. Express **12**, 3086 (2004)
8. J. Fulconis, O. Alibart, W. Wadsworth, P. Russell, J. Rarity, Opt. Express **13**, 7572 (2005)

9. J. Fan, A. Migdall, Opt. Express **15**, 2915 (2007)
10. J. Fan, A. Migdall, J. Chen, E.A. Goldschmidt, IEEE J. Sel. Top. Quantum Electron. **15**, 1724 (2009)
11. E.A. Goldschmidt, M.D. Eisaman, J. Fan, S.V. Polyakov, A. Migdall, Phys. Rev. A **78**, 013844 (2008)
12. J.A. Slater, J.S. Corbeil, S. Virally, F. Bussières, A. Kudlinski, G. Bouwmans, S. Lacroix, N. Godbout, W. Tittel, Opt. Lett. **35**, 499 (2010)
13. E. Brainis, Phys. Rev. A **79**, 023840 (2009)
14. P.S.J. Russell, J. Lightwave Technol. **24**, 4729 (2006)
15. J. Fan, A. Migdall, Opt. Express **13**, 5777 (2005)
16. W. Zhang, L. Xiao, L. Zhang, Y. Huang, J. Peng, Chin. Phys. Lett. **23**, 1201 (2006)
17. L. Xiao, W. Zhang, Y. Huang, J. Peng, Chin. Phys. B **17**, 995 (2008)
18. X. Li, P.L. Voss, J.E. Sharping, P. Kumar, Phys. Rev. Lett. **94**, 053601 (2005)
19. H. Takesue, K. Inoue, Phys. Rev. A **70**, 031802 (2004)
20. S.D. Dyer, M.J. Stevens, B. Baek, S.W. Nam, Opt. Express **16**, 9966 (2008)
21. Q. Lin, F.Y., G.P. Agrawal, Phys. Rev. A **75**, 023803 (2007)